Horizontal Calibration of Vessels with UASs

Casey O'Heran[a]* and Brian Calder[b]

[a]*Center for Coastal and Ocean Mapping and NOAA-UNH Joint Hydrographic Center, University of New Hampshire, Durham, NH, United States;* [b]*Center for Coastal and Ocean Mapping and NOAA-UNH Joint Hydrographic Center, University of New Hampshire, Durham, NH, United States.*

Corresponding Author:

Casey O'Heran, CCOM/JHC, University of New Hampshire, Chase Ocean Engineering Lab, 24 Colovos Road, Durham NH 03824, USA. Tel: +1 603 862 3438. Fax: +1 603 862 0839. E-mail: cto1004@wildcats.unh.edu.

Horizontal Calibration of Vessels with UASs

Knowledge of offset vectors from vessel mounted sonars, to systems such as Inertial Measurement Units (IMUs) and Global Navigation Satellite Systems (GNSS) is crucial for accurate ocean mapping applications. Traditional survey methods, such as employing laser scanners or total stations, are used to determine professional vessel offset distances reliably. However, for vessels of opportunity that are collecting volunteer bathymetric data, it is beneficial to consider survey methods that may be less time consuming, less expensive, or which do not involve bringing the vessel into a dry dock. Thus, this paper explores two alternative methods that meet this criterion for horizontally calibrating vessels.

UASs were used to horizontally calibrate a vessel with both Structure from Motion (SfM) photogrammetry and aerial lidar while the vessel was moored to a floating dock. Estimates of the horizontal deviations from ground truth, were obtained by comparing the horizontal distances between targets on a vessel, acquired by the UAS methods, to multiple ground truth sources: a survey-grade terrestrial laser scan and fiberglass tape measurements. The investigated methods were able to achieve horizontal deviations on the order of centimeters with the use of Ground Control Points (GCPs).

Keywords: Bathymetry; Crowdsourced Bathymetry; Unmanned Aerial Systems; Vessel Calibration; Remote Sensing

Subject classification codes:

Introduction

Modern technologies such as satellites and aircraft equipped with electromagnetic energy sensors (e.g., passive/active light and radar) and oceanographic vessels equipped with echo sounders, have become popular to map the seabed (Hillman, 2019), and are essential to effectively map the world ocean in the manner envisioned by the Seabed 2030 project (Mayer et al., 2018). With the immense amount of seafloor remaining unmapped, all potential sources of information have to be considered, including voluntary sources (Robertson, 2016) such as crowdsourced bathymetry (CSB).

CSB is the voluntary collection of depths measured by vessels equipped with standard navigation systems operating in routine maritime activities (Luma-ang, 2017; IHO, 2020). Anecdotally, however, in our examination of publicly available volunteer data (in this case the International Hydrographic Organisation's (IHO) Data Center for Digital Bathymetry CSB database), volunteer observers rarely, if ever, provide information on horizontal offsets between GNSS and echosounder systems, which lessens the value of the contributed observations. These ships are also unlikely to pay for offset surveys (Hughes Clarke, 2003) to be done, and even local sponsor organizations supporting the installation of data collection systems may not be able to provide either the equipment or expertise to conduct professional surveys (e.g., with a total station), depending on location and local capabilities. This process might in any case require the ship to be in dry dock, which we believe volunteer observers are unlikely to support. Alternative methods for survey are therefore required, ideally ones that can be taught readily to local support organizations and/or volunteer observers (albeit with the actual processing being done through centralized resources – at an IHO Trusted Node (IHO, 2018) for example – rather than locally).

Methods exist to estimate vertical offsets (Calder et al., 2020) with uncertainties on the order of 0.16m (one sigma), but non-traditional methods to estimate horizontal offsets between GNSS antenna and echo sounder(s) have not been reported. Survey-grade accuracy is likely not required for CSB purposes given the other limitations of the data (for the purposes of this work, we initially hypothesized order 30 cm lever arm uncertainty as a nominal goal that we would be willing to accept as "useful"), but in keeping with current hydrographic practice [IHO, 2020], it is important that uncertainties are minimized where possible in order to achieve any given level of bathymetric

measurement accuracy. Therefore, this paper focusses on alternative, approximate, techniques for horizontal calibration.

Development of Unmanned Aircraft Systems (UASs) for civilian based remote sensing applications has increased extensively over the last decade, leading to UASs achieving spatial mapping resolutions of 1-20 cm (Nebiker et al., 2008) using either (or both) high-definition digital cameras and light-weight scanning lidars. While lidars directly generate point clouds of range measurements, cameras collect a series of two-dimensional (2D) images to be processed by photogrammetric Structure from Motion (SfM) and multi-view stereo (MVS) algorithms, generating a three-dimensional (3D) model of the surveyed area (Snavely et al., 2008; Westoby et al., 2012; Schonberger and Frahm, 2016; Sanz-Ablanedo et al., 2018). Both UAS sensor types have demonstrated that they can quickly and efficiently map objects (Anderson and Gaston, 2013; Colomina and Molina, 2014; Simpson, 2018).

To examine the benefits and limits of the sensors for the current purpose, UAS surveys were performed over a moored/slightly moving vessel with many different configurations (e.g., with and without ground control) designed to elicit trade-offs in implementation. Applying both UAS sensors independently to determine the horizontal offsets on a single vessel allows an intercomparison of the ability of these methods to locate targets relative to the ship's reference frame, similar to that done by Simpson (2018), but for the application of mapping a slightly moving object.

Methods and Materials

The University of New Hampshire's (UNH) R/V *Gulf* Surveyor, a 48 ft length-over-all, twin-hull mapping research platform (see Figures 7-9 for approximate scales) was surveyed over six missions in 2019 with UASs at the UNH pier on New Castle Island, New Hampshire. (Full details of the data collection periods, and the cameras and

processing configurations are given in the supplemental materials.). A terrestrial laser scanner survey of the vessel, which was conducted in 2016 (Doucet Survey Inc., 2016) while on the hard and used to establish the ship's reference frame, was used to provide ground truth positions for the permanent survey monuments welded to the hull against which the estimates derived here were compared. The estimate of uncertainty in positions of the permanent monuments as established by this ground truth survey is 3mm (one sigma) (Doucet Survey Inc., 2016).

A control network consisting of ten Ground Control Points (GCPs) was used for each survey. For the lidar surveys, single frequency GNSS targets (AeroPoints) with post-processed positioning using the U.S. Continually Operating Reference Station (CORS) network were used; for UAS SfM surveys, nylon survey targets were laid and then occupied by a Trimble 5700 Geodetic receiver with a Zephyr antenna, for 10 minutes each, to establish their position. The control networks possess standard deviations on the millimeter levels, and were positioned in the World Geodetic System of 1984 (WGS84 (G1762)), which is aligned to the International Terrestrial Reference Frame (ITRF) of 2008 (ITRF2008).

A set of paper targets with center cut-outs to allow the ship monuments to be observed if required were also secured to the R/V *Gulf Surveyor* prior to each UAS experiment, allowing error estimates to be made by comparing the ground truth laser scanned distances between the five visible SRF monuments on the vessel to the optically reconstructed distances. Additionally, 12 unmodified targets were placed around the vessel's main and top decks. As a secondary source of error estimation, ground truth measurements between the SRF monuments and unmodified vessel targets were taken with fiberglass tape, Figure 1.

[Figure 1 near here]

Vertical control for water level changes was derived from the National Oceanic and Atmospheric Administration (NOAA) tide gauge at Fort Point, NH (Station ID 8423898), which is immediately adjacent to the survey site (NOAA, 2020).

UAS Structure from Motion

Structure from Motion Data Collection

Five separate days of UAS SfM missions were conducted to explore the practicality of performing horizontal vessel calibrations using UAS photogrammetry from a low-cost consumer grade UAS. A DJI Phantom 4 Pro was chosen for this study because it is inexpensive ($2,000 in 2019 US dollars), equipped with an IMU and consumer grade GNSS, has up to 30 minutes flight time, and includes a 20-megapixel camera (DJI, 2020).

Missions were conducted in grids parallel and orthogonal to the vessel's longitudinal axis ("3D grid") with nadir camera orientation; Pix4D Capture was used for data collection. Since high detail is desired for this type of survey, the amount of overlap between flight lines (side lap) and overlap between photos along a survey line (end lap) were both set to 90% of the frame. To investigate effects of flying height on accuracy, 21m and 31m above-ground-level (AGL) flights were conducted, resulting in Ground Sampling Distances (GSD) of 0.58 and 0.85cm/pixel, respectively.

Circular orbits with a 45° camera angle were also flown at 21m and 31m AGL to investigate whether the addition of oblique imagery would have an effect on the horizontal accuracies; oblique oriented elliptical flight paths following the along and across track directions of the vessel were flown at 31m AGL. Care was taken to minimize environmental variation across missions; camera properties were selected empirically to optimize apparent image quality, and survey flights were tide-coordinated to avoid excess vertical movement of the vessel. Camera adjustments (see supplemental materials, and

the following section) and UAS internal calibration (e.g., for IMU and compass) were carried out before each mission, along with inter-target measurements on the ship.

Since SfM relies on correspondences between frames of a static subject, wave-induced ship motion was expected to be a significant factor in overall accuracy. To study this effect, missions were conducted with the ship loosely moored to the dock using normal procedures, and then with extra spring lines to provide a more solid connection to the dock. Multiple missions were conducted in each configuration.

Structure from Motion Data Processing

Agisoft Metashape was used to perform camera calibrations, implement the SfM algorithm, and produce 3D point clouds, 3D surfaces, Digital Elevation Models (DEMs), and orthomosaics (Agisoft LLC, 2019). Camera calibration was conducted to avoid the error phenomenon known as "doming" (James et al., 2014), although extremely accurate calibration is not as essential for horizontal positioning as for vertical. Calibrations were computed for each flight and are available in the project files for each mission and configuration of data in the auxiliary materials.

The general processing workflow followed the one recommended and documented by the manufacturer (Agisoft LLC, 2019). However, with modelling a slightly moving object, alternate processing parameters were implemented in some instances. For example, disconnecting distortions in texturized mesh models were rectified by using the average blending method, which takes the weighted average of pixels over all relevant photographs (Agisoft LLC, 2019).

Final DEMs and orthomosaics were output in WGS84 (G1762) Universal Transverse Mercator (UTM) zone 19 North. Polylines were drawn on the orthomosaics, marking/measuring the observed Euclidian distances between the centers of vessel targets, Figure 2.

[Figure 2 near here]

All 21m and 31m 3D grid flights were processed individually. Subsequently, each individual 3D grid dataset was processed with and without GCPs in three modes: once using the maximum number of GCPs in the coverage area (between eight and ten, depending on the final drone flight path), once with four, and once with three GCPs. Processing sections were also constructed by combining multiple missions. Grids at 31m were combined with a 21m oblique orbit for all individual missions in which an oblique orbit was flown. To investigate the effect of masking, two 3D grid datasets were masked to execute the SfM algorithm solely based on the location of the vessel. However, masking content outside the vessel excluded the pier based GCPs, thus preventing accurate georeferencing of the masked data. In total, over 30 sections of data were processed to produce dozens of point clouds, 3D meshes, DEMs, and orthomosaics.

UAS Lidar

UAS Lidar Data Collection

A UAS lidar survey of the R/V *Gulf Surveyor* was conducted by ARE Ltd. on April 17, 2019 using a DJI Matrice 600 Pro with RTK positioning (DJI, 2020), and a Riegl miniVUX scanning system capable of collecting at 100kHz. For non-vegetated areas, this system is capable of achieving nominal absolute accuracies of approximately 2-3 cm horizontal Root Mean Square Error (RMSE) and 4-6 cm RMSEz (ARE, 2019). To provide accurate Post Processed Kinematic (PPK) GNSS corrections to the UAS trajectory, a CHC X900R static GNSS base station was set up on the National Geodetic Survey (NGS) control point AB2631 (NGS, 2020), located just southwest of the site (43° 04’ 15.17437” N, 070° 42’ 48.58831” W). Static GNSS observations on the control point began approximately half an hour before the mission was conducted and concluded half

an hour after the mission ended. Ten AeroPoints were used as check points for the final georeferenced lidar model.

The flight pattern consisted of three lines parallel to the R/V *Gulf Surveyor's* along track direction, in addition to three lines parallel to the vessel's across track orientation. This 3D grid pattern was repeated at 46m, 31m, and 16m AGL. A final "detail" pass was flown at 10-meters AGL parallel to the ship's across track direction. Along track line lengths spanned the entire length of the pier, while lengths of the across track lines ranged from the north side of the pier to land directly south of the pier. Survey passes were flown at 2-3m/s resulting in approximately 120 points/m^2 directly underneath the aircraft's flight path over a single pass. In total, the survey took approximately 19 minutes to conduct in 19 passes.

UAS Lidar Data Processing

Initial processing of the lidar and associated GNSS observations were performed by ARE. Novatel Inertial Explorer v8.70 was used to perform the post processing of the aircraft trajectory. Scan angles for the lidar data were left at ± 90° from the nadir beam so that the lower altitude passes would enable data returns from higher angles. The lidar datasets were processed to meet the American Society of Photogrammetry and Remote Sensing (ASPRS) "Positional Accuracy Standards for Digital Geospatial Data" (2015) for a 2.5 (cm) RMSEx / RMSEy Horizontal Accuracy Class, which is equivalent to a Positional Horizontal Accuracy of ±6.1 cm (95% CI), and to achieve a 5 cm RMSEz Vertical Accuracy Class, equating to a Non-vegetated Vertical Accuracy (NVA) of ±9.8cm (95% CI). ARE's RMSEz calculations against the nine AeroPoints in the coverage area demonstrate an RMSEz value of 1.006 cm (ARE, 2019). ARE provided the trajectory results, point cloud (LAS) files, and a report of survey. The LAS files were provided in

the State Plane Coordinate System of 1983 (SPCS83) (NAD83 (NSRS2007)), New Hampshire zone, FIPS 2800, with units of US survey feet (sft) and orthometric heights in NAVD88 (Geoid12B) US survey feet.

The LAS files were brought into Global Mapper (version 19.1), and SRF monuments were identified in the colorized point cloud for ground-truth comparison. Due to a data capture fault, images from the lidar scanner equipped UAS were not available to colorize the points, so images from the UAS SfM at 31m (April 17, 2019) processed with three GCPs, was overlaid onto the lidar point cloud to provide true color. To prepare the lidar model for accuracy assessment, polylines were drawn in the Global Mapper 2D viewer between the centers of the vessel targets.

Horizontal Error Estimation

Horizontal magnitude deviations for the UAS lidar and SfM models were calculated by subtracting the respective ground truth lengths from the observed lengths in the local level reference frame. Comparisons were broken up into primary and secondary forms. Primary comparisons involved the differences between the ground truth laser scanned monument distances and the observed UAS lidar/SfM monument distances. Secondary comparisons were between the ground truth fiberglass tape measurements of vessel targets and the observed UAS lidar/SfM vessel target distances. The laser scan survey took priority as the primary ground truth source due to its higher accuracy.

For the final lidar model, distances were taken from the polylines between vessel targets in the 2D viewer of Global Mapper; for the SfM models, measurements were taken from the orthomosaics. In total, there were 10 primary baselines and 17 secondary baselines for each observed model. Differences, the average differences for each component set, and a sample standard deviation

$$\sigma = \sqrt{\frac{\sum(X-\overline{X})^2}{n-1}} \quad (1)$$

was computed for each respective set of differences, and a standard error (SE),

$$\text{SE} = \frac{\sigma}{\sqrt{n}} \quad (2)$$

was then derived. Finally, an expanded uncertainty for each model,

$$U = SE \cdot CF \quad (3)$$

was computed, using a coverage factor (CF) at 95% CI based on nine and sixteen degrees of freedom for primary and secondary comparisons, respectively.

Directionality of modelled to ground-truth offset deviations was determined by affine transforming the local level coordinates for the monuments and targets into the SRF using the monuments as reference markers. Cartesian differences in the SRF were then computed.

The Euclidian distances between monuments, Cartesian deviation vectors in the SRF, and deviation magnitudes for each baseline were calculated. In addition, absolute scales,

$$S_x = \left|\frac{L_{x\,Observed}}{L_{x\,Ground\,Truth}}\right| \quad (4)$$

$$S_y = \left|\frac{L_{y\,Observed}}{L_{y\,Ground\,Truth}}\right| \quad (5)$$

for each Cartesian baseline in the SRF were calculated.

Results

Vessel Motion Analysis

Initial missions were conducted during a period of high tidal change (approximately 3m total variation between high and low tide over six hours)**,** resulting in feature duplication within the point cloud when combining two separate photogrammetry missions, Figure 3, which indicates a vertical displacement threshold in Agisoft Metashape. To eliminate this phenomenon, all other missions were conducted during high or low tide (variations less than 0.1m over the mission).

[Figure 3 near here]

Loose vessel configurations also resulted in visual distortions and blurring in the associated orthomosaic, unlike those from tight vessel configurations. Examination of the attitude data collected from the POS/MV 320 installed on the *Gulf Surveyor* during the transition from loose to tight configurations, Figure 4, demonstrates that heading experiences the most change, going from an overall range of ±1° to ±0.6° over 15s intervals. Analysis of the shift of the bow-most SRF monument within 15s intervals shows shifts diminishing from 0.05-0.20m to <0.07m suggesting heading changes cause the blurriness in the orthomosaics. Control of heading through mooring lines is therefore significant in reliable orthomosaic construction, and therefore offset estimation.

[Figure 4 near here]

Error Analysis

Figure 5 displays the estimated horizontal deviations for all processed datasets in which the primary ground truth data was used, demonstrating that the SfM models without GCPs consistently result in decimeter and sometimes centimeter level deviation ranges. SfM models processed with GCPs show deviation ranges on the centimeter level, and both

average distance differences and deviation ranges, in most cases, lessen when GCPs are implemented. The lidar survey resulted in similar centimeter level deviation ranges (mean 0.01 ± 0.017 m at 95% CI). These observations demonstrate that the inclusion of GCPs will result in consistent SfM survey qualities, on a par with lidar-based surveys, while non-GCP models produce, at times, inconsistent results. This is due to the consumer-grade GNSS receiver used for SfM flights when unaided by survey-grade GCP observations. Higher quality GNSS observations during capture could result in more reliable scaling of the models, which is an observable problem with the current results (without GCPs). The deviations indicate no significant change between different flying heights, or when going from implementing the maximum number of GCPs to three or four.

[Figure 5 near here]

The loose vessel configurations in the last two sections of Figure 5 mostly possess higher deviation ranges compared to their tight vessel configuration counterparts, which is caused by differences in the heading change of the vessel, as demonstrated previously. When GCPs are implemented in this scenario the deviation ranges shrink significantly. Analogous result patterns are experienced for deviation estimates achieved when comparing observed measurements to secondary ground truth data, Figure 6. It is important to note that primary comparisons most likely represent the best-estimated horizontal deviations from the ground truth due to its higher accuracy ground truth measurements.

[Figure 6 near here]

Figures 7 demonstrates the size and direction of the deviations in the SRF when using primary ground truth data, and particularly a tendency for the deviations to point towards the starboard side of the vessel. For tight vessel configurations, this is likely

because the control network is located on the pier, to the starboard side of the vessel. Similar datasets without GCPs show analogous, but not as dominant directional biases, suggesting a slight deviation bias towards fixed content in the form of the pier. For a loose vessel configuration, Figure 8, larger errors are observed, and suggest a more randomly distributed deviation direction pattern when implementing GCPs. These differences are due to magnitude of vessel motion.

[Figure 7 near here]

[Figure 8 near here]

Figure 9 shows that adding GCPs reduces baseline under-scaling; loose vessel configurations experienced similar scaling re-distribution when including GCPs. Note that lines shown going off the plots represent baselines that are predominantly aligned with an axis. Thus, if the estimated baseline distance for the direction not aligned with an axis (baseline distance close to zero) is slightly different from ground truth, the scale for that respective direction will be erroneously exaggerated.

[Figure 9 near here]

Discussion

The UAS SfM photogrammetry datasets observed here experienced decimeter and occasionally centimeter level deviation estimates without ground control. Inclusion of ground control for the UAS SfM photogrammetry datasets lead to consistent centimeter level results, even with just three or four GCPs; UAS lidar also experienced a deviation on the centimeter level. Additional SfM techniques such as masking and combining nadir with oblique imagery without GCPs appear to have small effects on deviation estimates, while altering flying height had no clear impact on deviations.

The methods discussed here present a choice between SfM photogrammetry and lidar scanning as modalities for relative positioning of targets on a vessel of opportunity,

with some overlapping and separate factors to consider. Table 1 highlights the trade-offs between using SfM photogrammetry and lidar scanning for horizontal vessel calibrations. The results express a spectrum of complexity and accuracy of survey, from the SfM survey without GCPs to lidar scanning or SfM with GCPs. The lower-cost instruments used for SfM can achieve performance comparable to lidar scanning, although the overall cost of the survey depends on many other factors such as processing time, etc. Use of consumer-grade software and hardware for SfM, however, rather than specialist systems (for lidar scanning) and the potential for centralized processing suggest that there may be advantages in the SfM approach for the target application of determining positions on volunteer vessels of opportunity by non-expert observers.

[Table 1 near here]

Conducting the experiments provided some insights into successful estimation. Specifically, it is best to perform the survey(s) at high or low tide, with the vessel tied down as tightly as possible, and during calm environmental conditions. For consistent centimeter level accuracies, a ground control network near the vessel is required (RTK positioning is also possible, but was not studied here), but this research demonstrated that it was not essential to have the vessel reside within the control network to obtain centimeter level accuracies: simply having the control network as close to the vessel as possible is enough. If large vessel movement is expected, it is recommended to utilize GCPs to limit the errors introduced from the motion. However, this protocol will not eliminate all induced errors and the error directionalities will become more random with higher degrees of motion. If imagery used to colorize lidar data is collected separately from the lidar scanning (as done here), uncertainty will most likely be introduced into the lidar data due to differences in vessel motion between the two collection efforts. Additionally, if the vessel does not have an established SRF, the workflow outlined in

this paper could be used to establish the SRF and refer coordinates to it; a point in the middle of the vessel that can be seen from the aircraft should be chosen as the arbitrary horizontal origin of the vessel if one does not already exist. If the echo sounder is not visible from the aircraft, a point from which manual measurements to the echo sounder can be made could be established. Auxiliary oblique-oriented flights should be considered if vertical calibrations are contemplated.

Conclusion

The purpose of this research was to determine the extent to which non-traditional survey techniques could be used to position points on a volunteer ship of opportunity which would otherwise be unlikely to have a well-established position system with which to determine offsets between the various instruments used to generate volunteered geographic information. The experiments conducted demonstrated that it appears to be possible, with minimal ground control, to determine positions on a floating vessel to within a few centimeters (order 0.005±0.01m [95%] at best to 0.01±0.02m [95%] at worst, Figure 5, over a 14.6m [48ft] vessel length) compared to a terrestrial laser scan of the vessel, while results with no GCPs generated positions to order a decimeter (order 0.12±0.05m [95%] in some cases, Figure 5). The experiments also demonstrated that the performance of structure from motion photogrammetry using a retail-level drone's built-in camera were comparable to that of a UAS lidar scanner (in both cases with GCPs), given suitable experimental conditions (e.g., ensuring that the vessel was secured to the dock as well as possible with extra lines, and surveying over either high or low tide to avoid vertical offsets during the mission). These results suggest that UAS-based survey is a practical alternative to traditional land surveying methods for point positioning on floating volunteer ships of opportunity, and therefore in determining horizontal offsets for subsequent data correction.

Acknowledgments

This work was supported by the National Oceanic and Atmospheric Administration (NOAA) under Grant NA15NOS4000200 to the Joint Hydrographic Center at the University of New Hampshire. The authors would like to thank the Captain and crew of the R/V *Gulf Surveyor* for their help throughout the data collection process.

Declaration of Interest

The data supporting the conclusions of this article are included within the article. Any questions regarding these data can be directed to the corresponding author.

References

American Society for Photogrammetric Engineering and Remote Sensing (ASPRS). (2015). ASPRS positional accuracy standards for digital geospatial data (Edition 1, Version 1.0., November, 2014). Photogrammetric Engineering & Remote Sensing, 81(3), A1-A26.

Anderson, Karen, and Kevin J. Gaston (2013). Lightweight unmanned aerial vehicles will revolutionize spatial ecology. Frontiers in Ecology and the Environment 11, no. 3: 138-146.

Agisoft LLC. (2019). Agisoft Metashape User Manual Professional Edition, Version 1.5. Available at: https://www.agisoft.com/pdf/metashape-pro_1_5_en.pdf

ARE. (July 2019). UNH Gulf Surveyor Lidar Scan. For access contact info@ccom.unh.edu.

Calder, Brian R., Semme J. Dijkstra, Shannon Hoy, Kenneth Himschoot, and Andrew Schofield. (2020). A Design for a Trusted Community Bathymetry System. *Marine Geodesy*: 1-32.

Colomina, Ismael, and Pere Molina (2014). Unmanned aerial systems for photogrammetry and remote sensing: A review. ISPRS Journal of photogrammetry and remote sensing 92: 79-97.

DJI. Matrice 600 Pro. Retrieved on January 20, 2020. Retrieved from: https://www.dji.com/matrice600-pro

DJI. Phantom 4 Pro. Retrieved on January 20, 2020. Retrieved from: https://www.dji.com/phantom-4-pro/info

Doucet Survey Inc. (May 2016), Surveying and Laser Scanning Service For the "Gulf Surveyor" Research Vessel. For access contact info@ccom.unh.edu.

Doucet Survey Inc. (June 2016), Updated Reference Coordinates For the "Gulf Surveyor" Research Vessel. For access contact info@ccom.unh.edu.

Hillman, J. I. (2019). Mapping the Oceans. *Frontiers for Young Minds*, *7* (Article 25).

Hughes Clarke, John. 2003. A reassessment of vessel coordinate systems: what is it that we are really aligning. In *US Hydrographic Conference*.

IHO. Crowdsourced Bathymetry. Retrieved on January 20, 2020. Retrieved from: https://iho.int/en/crowdsourced-bathymetry

IHO (2020). Standards for Hydrographic Surveys (S.44), 6.0.0 Ed. Retrieved on January 5, 2021. Retrieved from: https://iho.int/uploads/user/pubs/Drafts/S-44_Edition_6.0.0-Final.pdf.

James, Mike R., and Stuart Robson. (2014). Mitigating systematic error in topographic models derived from UAV and ground-based image networks. *Earth Surface Processes and Landforms* 39, no. 10: 1413-1420.

Luma-ang, Carter. (2017). Crowdsourced Bathymetry: Supporting Progress or Threatening Security. https://maritimereview.ph/crowdsourced-bathymetry-supporting-progress-or-threatening-security/

Mayer, Larry, Martin Jakobsson, Graham Allen, Boris Dorschel, Robin Falconer, Vicki Ferrini, Geoffroy Lamarche, Helen Snaith, and Pauline Weatherall. (2018). The Nippon Foundation—GEBCO seabed 2030 project: The quest to see the world's oceans completely mapped by 2030. *Geosciences* 8, no. 2: 63.

Nebiker, Stephan, Adrian Annen, Marco Scherrer, and David Oesch. (2008). A light-weight multispectral sensor for micro UAV—Opportunities for very high resolution airborne remote sensing. *The international archives of the photogrammetry, remote sensing and spatial information sciences* 37, no. B1: 1193-1199.

NGS. National Geodetic Survey Data Explorer. Retrieved on January 20, 2020. Retrieved from: https://www.ngs.noaa.gov/NGSDataExplorer/

NOAA. Tides/Water Levels. Retrieved on January 20, 2020. Retrieved from: https://tidesandcurrents.noaa.gov/waterlevels.html?id=8423898&units=metric&bdate=20190417&edate=20190418&timezone=LST/LDT&datum=MLLW&interval=6&action=

Robertson, Evan. (2016). Crowd-sourced Bathymetry Data via Electronic Charting Systems. In *ESRI Ocean GIS Forum*.

Sanz-Ablanedo, Enoc, Jim H. Chandler, José Ramón Rodríguez-Pérez, and Celestino Ordóñez. (2018). Accuracy of unmanned aerial vehicle (UAV) and SfM

photogrammetry survey as a function of the number and location of ground control points used. *Remote Sensing* 10, no. 10: 1606.

Schonberger, Johannes L., and Jan-Michael Frahm (2016). Structure-from-motion revisited. In Proceedings of the IEEE Conference on Computer Vision and Pattern Recognition, pp. 4104-4113.

Simpson, Chase H. (2018). A Multivariate Comparison of Drone-Based Structure from Motion and Drone-Based Lidar for Dense Topographic Mapping Applications. Master's thesis, Oregon State University.

Snavely, Noah, Steven M. Seitz, and Richard Szeliski (2008). Modeling the world from internet photo collections. International Journal of Computer Vision 80, no. 2: 189-210.

Westoby, Matthew J., James Brasington, Niel F. Glasser, Michael J. Hambrey, and Jennifer M. Reynolds (2012). Structure-from-Motion "photogrammetry": A low cost, effective tool for geoscience applications. Geomorphology 179: 300-314.

Word Count: 4866

Tables and Figures

UAS Trade-offs: Vessel Calibration Surveys	
UAS SfM Photogrammetry	**UAS Lidar**
Low cost UAS and camera sensors can be utilized	Expensive UAS and lidar units required
Decimeter/centimeter level accuracies without GCPs	High quality aircraft positioning required (RTK or PPK GNSS)
Centimeter level accuracies with GCPs	Centimeter level accuracies
Quick survey time. Multiple flights may be required	Quick survey time. A single flight is most likely sufficient
Survey quality affected by water level and vessel attitude change	Survey quality affected by water level and vessel attitude change
Requires extra lines to tie down the vessel, optimizing survey qualities	Requires extra lines to tie down the vessel, optimizing survey qualities
Best performed during high or low tide	Best performed during high or low tide
Simple to operate	Complex to operate

Table 1. An illustration showing the trade-offs between the two investigated UAS methods for horizontally calibrating vessels.

Figure 1. Ground control and measurement targets for the experiments on the R/V Gulf Surveyor: unmodified vessel targets (green), SRF points (purple), and three of the ten GCPs (red). The remaining GCPs were spread out along the length of the adjacent pier, alternating sides as shown.

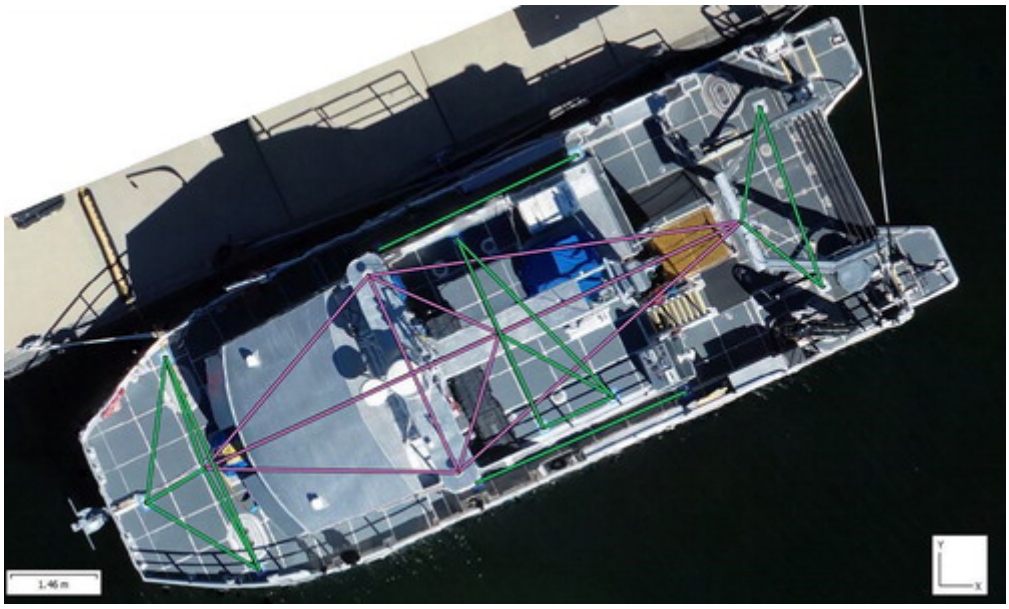

Figure 2. Orthomosaic of R/V Gulf Surveyor made from photographs taken on 17 April 2019. Purple polylines represent measurements between SRF monuments, and green polylines represent measurements between vessel targets.

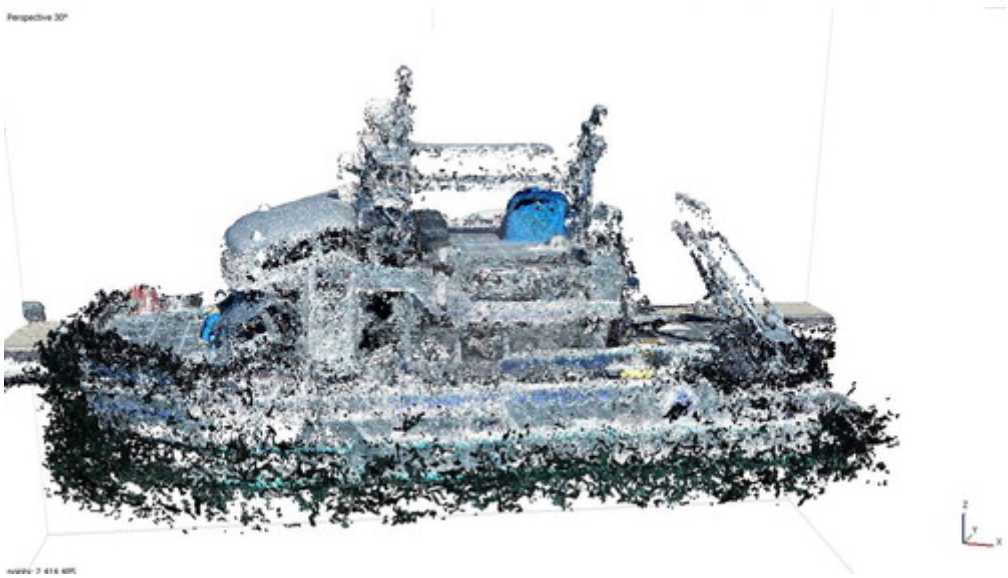

Figure 3. Point cloud generated from two 3D grid flights collected on 17 April 2019 during a falling tide, leading to vertical "doubling" of points due to thresholding effects in Metashape.

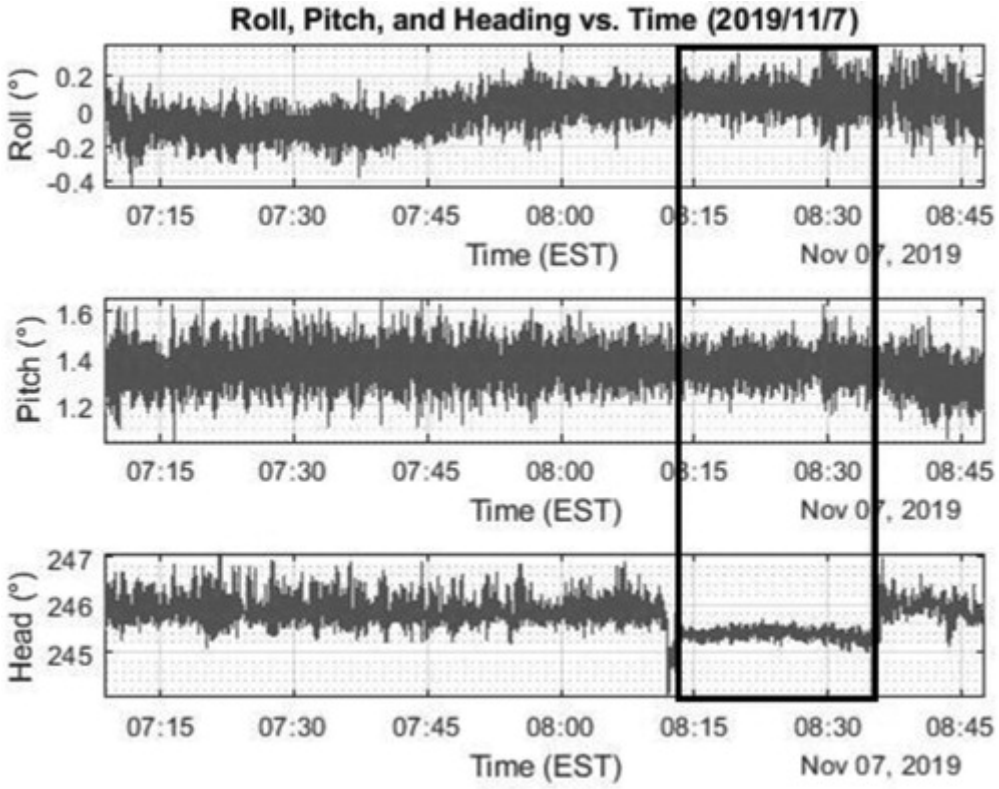

Figure 4. Roll, pitch, and heading time series of the R/V Gulf Surveyor loosely and tightly tied down on 7 November 2019. The black rectangle represents the time in which the vessel was tied down tight.

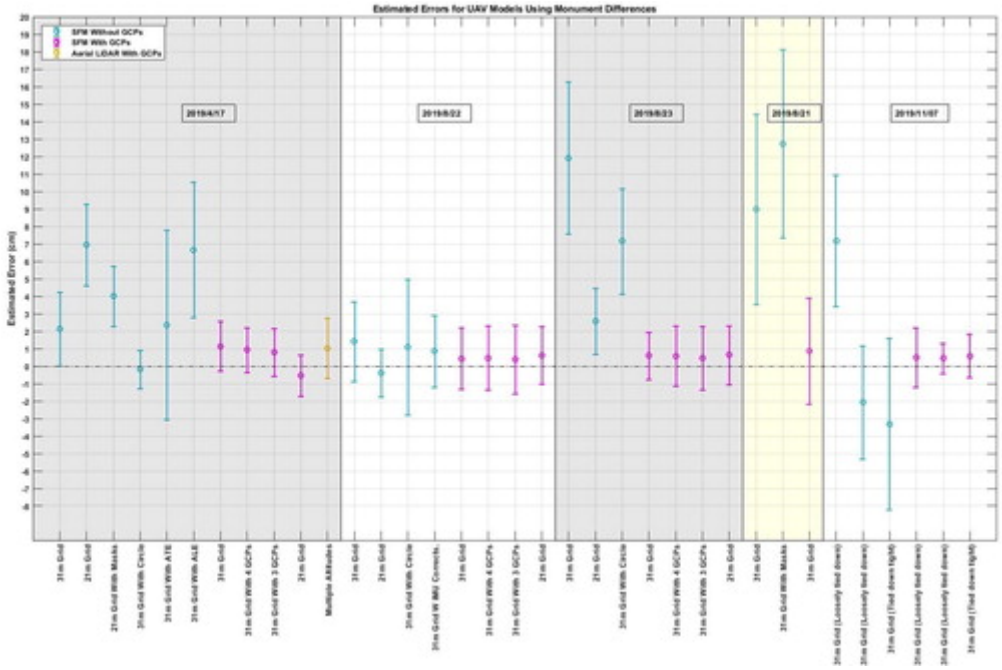

Figure 5. General deviation estimates for all UAS surveys utilizing the primary source data as ground truth. Deviation ranges are represented by the combination of the mean difference (circles) and expanded uncertainty (error bars) for each dataset.

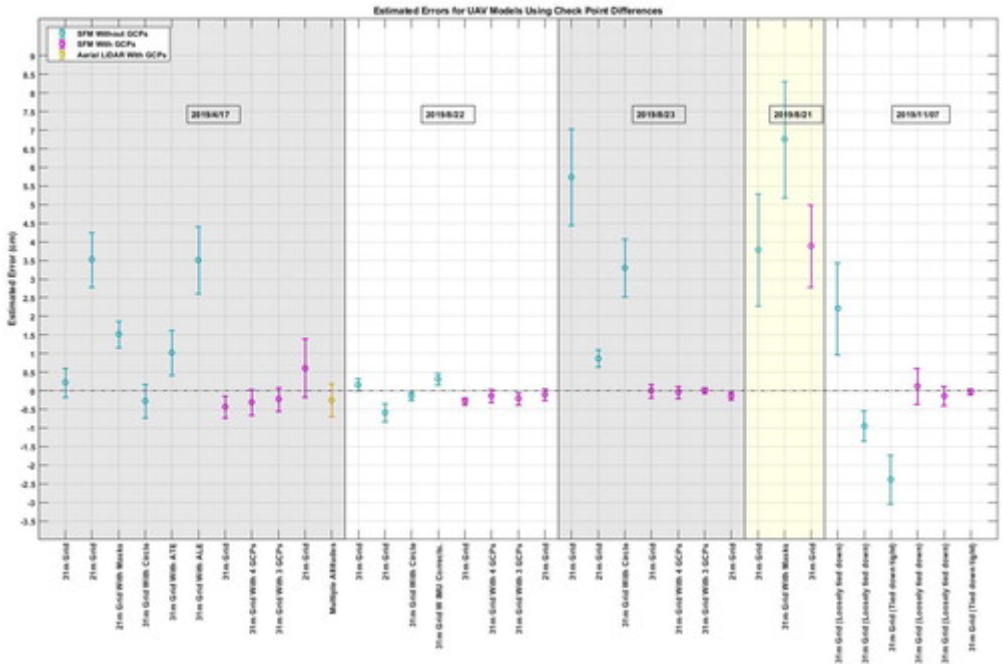

Figure 6. General deviation estimates for all UAS surveys utilizing the secondary source data as ground truth. Deviation ranges are represented by the combination of the mean difference (circles) and expanded uncertainty (error bars) for each dataset.

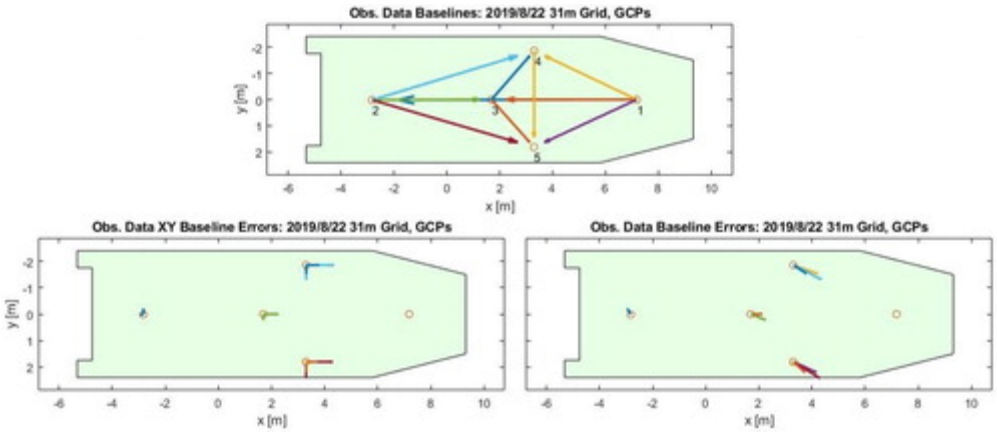

Figure 7. SRF baseline lengths (top), error vectors (left), and polar errors (right) of a 31 m grid GCP dataset (tight vessel configuration) flown on 22 August 2019. Errors are scaled by a factor of 30.

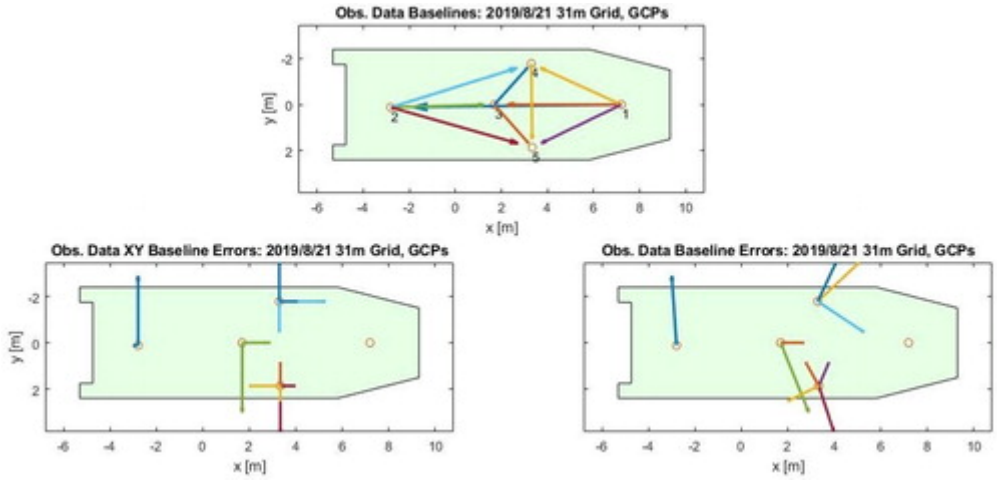

Figure 8. SRF baseline lengths (top), error vectors (left), and polar errors (right) of a 31 m grid GCP dataset (loose vessel configuration) flown on 21 August 2019. Errors are scaled by a factor of 30.

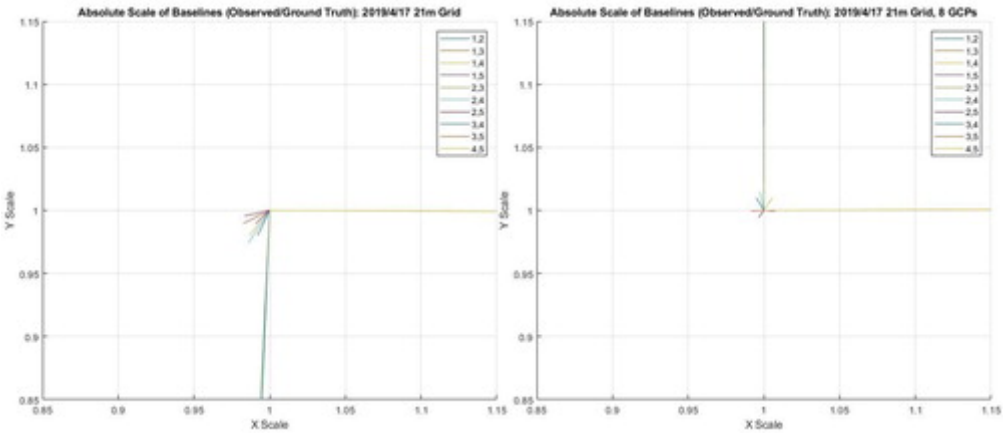

Figure 9. Absolute scales of SRF baselines observed from a 21 m grid flown on 17 April 2019 without GCPs (left) and with GCPs (right).

Models Generated for Analysis

A total of 35 individual digital models (point clouds and orthomosaics) were generated from the experiments using different combinations of flying heights and trajectories (i.e., grids over the ship, or circular or elliptical trajectories around the ship to provide oblique details). In addition, ground control points (GCP) were laid out before the experiments, and the data were processed with varying numbers of GCPs (including the case with no GCPs) to investigate the trade-off in computation and accuracy achievable. The details of the combinations, and source data, are provided below. Project files (for Agisoft Metashape) for the results reported in the manuscript, which include calibration parameters, are provided as a separate ZIP file.

UAS Collection Day	Processing Classification
Wednesday, April 17, 2019 Vessel tied down tight	31m grid 21m grid 21 grid with Masks 31m grid with circle 31m grid with across track ellipse 31m grid with along track ellipse 31m grid (Eight GCPs) 31m Grid (Four GCPs) 31m Grid (Three GCPs) 21m grid (Eight GCPs) LiDAR
Wednesday, August 21, 2019 Vessel tied down loosely	31m grid 31m grid with masks 31m grid (10 GCPs)
Thursday, August 22, 2019 Vessel tied down tight	31m grid 21m grid 31m grid with circle 31m grid with IMU corrections 31m grid (10 GCPs) 31m grid (Four GCPs) 31m grid (Three GCPs) 21m grid (Eight GCPs)
Friday, August 23, 2019 Vessel tied down tight	31m grid 21m grid 31m grid with circle 31m grid (10 GCPs) 31m grid (Four GCPs) 31m grid (Three GCPs) 21m grid (10 GCPs)
Thursday, November 7, 2019	31m grid A (Vessel tied down loosely) 31m grid B (Vessel tied down loosely) 31m grid C (Vessel tied down tight) 31m grid A (10 GCPs) 31m grid B (10 GCPs) 31m grid C (10 GCPs)

Lidar Flightpath Details

The survey of the R/V Gulf Surveyor with lidar was conducted by ARE Ltd. on April 17, 2019 using a DJI Matrice 600 Pro with RTK positioning (and a local ground station), and a Riegl miniVUX lidar. AeroPoint GCPs were used. The details of the flight lines are provided below.

Survey Pass Number	AGL Altitude (m)	Line Direction	Line Position
1	46	Stern to bow	Offset from center of vessel
2	46	Bow to stern	Centerline
3	46	Stern to bow	Offset from center of vessel
4	46	Port to starboard	Offset from center of vessel
5	46	Starboard to port	Centerline
6	46	Port to Starboard	Offset from center of vessel
7	31	Starboard to port	Offset from center of vessel
8	31	Port to starboard	Centerline
9	31	Starboard to port	Offset from center of vessel
10	31	Stern to bow	Offset from center of vessel
11	31	Bow to stern	Centerline
12	31	Stern to bow	Offset from center of vessel
13	15	Bow to stern	Offset from center of vessel
14	15	Stern to bow	Centerline
15	15	Bow to stern	Offset from center of vessel
16	15	Starboard to port	Offset from center of vessel
17	15	Port to starboard	Centerline
18	15	Starboard to port	Offset from center of vessel
19	10	Port to starboard	Centerline